Transient Incomplete Separation of Species with Close Diffusivity to Study the Stability of Affinity Complexes

Tong Ye Wang, Jean-Luc Rukundo, An T. H. Le, Nikita A. Ivanov, J. C. Yves Le Blanc, Boris I. Gorin, and Sergey N. Krylov*

Cite This: *Anal. Chem.* 2022, 94, 15415−15422

Read Online

ACCESS | 📊 Metrics & More | 📑 Article Recommendations | 🆘 Supporting Information

ABSTRACT: Large molecules can be generically separated from small ones, though partially and temporarily, in a pressure-driven flow inside a capillary. This transient incomplete separation has been only applied to species with diffusion coefficients different by at least an order of magnitude. Here, we demonstrate, for the first time, the analytical utility of transient incomplete separation for species with close diffusion coefficients. First, we prove *in silico* that even a small difference in diffusivity can lead to detectable transient incomplete separation of species. Second, we use computer simulation to prove that such a separation can be used for the reliable determination of equilibrium dissociation constant (K_d) of complexes composed of similar-sized molecules. Finally, we demonstrate experimentally the use of this separation for the accurate determination of K_d value for a protein−aptamer complex. We conclude that "accurate constant via transient incomplete separation" (ACTIS) can serve as a reference method for affinity characterization of protein−aptamer binding in solution.
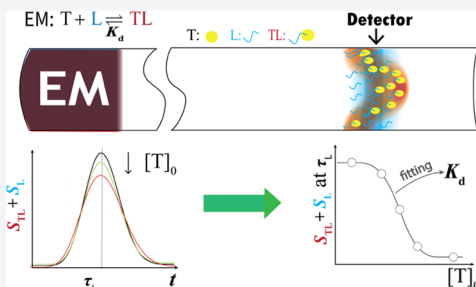
Affinity interaction of molecules plays important roles in technology and biology.[1−4] A ligand (L) binds a target (T) noncovalently and reversibly to form a target−ligand complex (TL):[5,6]

$$T + L \underset{K_d}{\rightleftharpoons} TL \tag{1}$$

The strength of this complex is characterized by the equilibrium dissociation constant K_d (the lower the K_d value the tighter the complex):

$$K_d = \frac{[T]_{eq}[L]_{eq}}{[TL]_{eq}} \tag{2}$$

where $[T]_{eq}$, $[L]_{eq}$, and $[TL]_{eq}$ are the equilibrium concentrations of the unbound target, unbound ligand, and the complex, respectively. Knowing accurate K_d values is pivotal to the development of diagnostics and therapeutics as well as understanding of cellular processes.[7−9]

Established methods for determining K_d fall into five major categories: spectroscopic, biosensoric, calorimetric, thermophoretic, and electrophoretic.[10−13] Each category has its unique sources of inaccuracy, which, in turn, lead to discrepancies between the results obtained from different methods for the same complex. Sometimes, quantitative disagreements are so drastic that different qualitative conclusions are made: one group of researchers reports binding, while the other claims no binding.[14]

The roots of the inaccurate K_d problem are not technical but fundamental. Unlike common physical values, such as mass,

time, and length, which have reference standards, there are no reference reactions with reference K_d values. It appears to be an axiom that the lack of a reference reaction forbids creating a reference method for K_d determination. This axiom has been challenged recently by a demonstration that the accuracy of an analytical method can be tested and characterized *in silico* if the method is deterministic. A deterministic method is the one that can be described comprehensively by a system of partial differential equations and, therefore, a virtual instrument can be created, and virtual experiments can be conducted with virtual reference-standard samples.[15−18]

The first deterministic method for finding K_d values of protein−small-molecule complexes has been recently introduced and termed "accurate constant via transient incomplete separation" (ACTIS).[19] ACTIS is based on very fast (typically achieved in less than 1 min) transient incomplete separation (TIS) of the complex from the small molecule. TIS of two species always occurs in a pressure-driven laminar flow inside a capillary if their diffusion coefficients differ.[20−24] The concept of ACTIS is reiterated in Figure 1. An equilibrium mixture (EM) of the target and ligand is prepared in an incubation buffer outside of the capillary. The mixture contains T, L, and
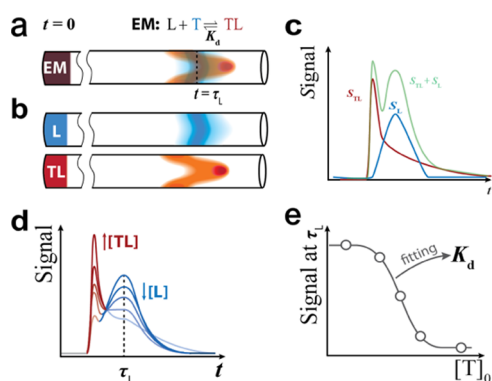
Figure 1. Concept of ACTIS. (a) A sample plug of the equilibrium mixture (EM) of T, TL, and L is injected in a capillary prefilled with the pure buffer and propagated by a pressure-driven flow. (b) The different flow velocities across the capillary and different rates of transverse diffusion of TL and L cause the separation of TL from L in the longitudinal direction. (c) The detector registers both the free ligand and the target-bound ligand indiscriminately and produces their cumulative signal. The dependence of this signal on time (a separagram) is comprised of two overlapping peaks: a nondiffusive peak of the target-bound ligand and a diffusive peak of free ligand. (d) A set of separagrams corresponding to different values of $[T]_0$ is generated. (e) A classic binding isotherm "R versus $[T]_0$" is built. The values of the fraction of free ligand, $R = [L]_{eq}/[L]_0$, are calculated from signals at time τ_L taken from the separagrams for different $[T]_0$. The K_d value is obtained from fitting the binding isotherm "R versus $[T]_0$" with the theoretical dependence of R on $[T]_0$, where K_d is the fitting parameter.

TL at their equilibrium concentrations linked by K_d according to eq 2. A sample plug of this mixture is injected into a capillary prefilled with the pure buffer solution. TIS of TL from L is achieved when this plug is propagated inside the capillary by a pressure-driven flow. Such a flow has a parabolic flow-velocity profile (Figure 1a). The maximum flow velocity, v_{max}, is in the center of the capillary, the zero velocity is on the capillary walls, and the average flow velocity is $v_{av} = v_{max}/2 = Q/(\pi a^2)$, where Q is the volumetric flow rate and a is the inner radius of the capillary. The interplay between different flow velocities across the capillary and different rates of transverse diffusion of TL and L causes separation of TL from L in the longitudinal direction (Figure 1b). This separation is fast but incomplete: the zones of TL and L always overlap. This separation is also transient: it extends to maximum when the propagation time reaches the characteristic time of diffusion of the ligand (τ_L) from the capillary center to its wall, and it gradually dissipates with longer propagation. If the diffusion coefficient of the ligand μ_L is known, τ_L can be calculated as a^2/μ_L. To propagate the plug to the detector at time τ_L, Q is chosen so that v_{av} is linked to the distance l inside the capillary from the point of start of TIS to the detector as $v_{av} = l/\tau_L$. The detector is set to detect the ligand, and it produces a cumulative signal from both the target-bound ligand and free ligand. The dependance of this signal on time is called a "separagram", which is comprised of two overlapping peaks: a nondiffusive peak of target-bound ligand complex and a diffusive peak of free ligand (Figure 1c, left). The detector does not distinguish target-bound ligand from free ligand and, therefore, the separagram is a sum of the diffusive and nondiffusive peaks (Figure 1c, right). To determine K_d, TIS is performed for a series of equilibrium mixtures with a constant total concentration of ligand, $[L]_0 = [L]_{eq} + [TL]_{eq}$, and a

varying total concentration of target, $[T]_0 = [T]_{eq} + [TL]_{eq}$. Accordingly, a set of separagrams corresponding to different values of $[T]_0$ is generated (Figure 1d). Signals at time τ_L are taken from these separagrams to calculate the fractions of free ligand, $R = [L]_{eq}/[L]_0$, for different $[T]_0$. The R values are used to build a classic binding isotherm "R versus $[T]_0$", which, in turn, reveals the value of K_d when fitted with the theoretical dependence of R on $[T]_0$ (Figure 1e).[19] Its accuracy has been proven *in silico*, and it has been shown that an accurate ACTIS instrument could be constructed.[25]

There is a universally accepted view that TIS is only applicable to species greatly different in size. Therefore, all examples of TIS in the literature relate to species, which differ in the diffusion coefficient by a factor of 10 or more.[20−26] Such a predisposition made previous ACTIS efforts to focus on protein−small-molecule complexes (diffusion coefficients of a small molecule and a protein−small-molecule complex differ by approximately a factor of 10). The goal of this work was to understand if the TIS of protein−large ligand complex from the unbound ligand could be detected and used for K_d determination for such complexes.

■ MATERIALS AND METHODS

Chemicals, Materials, and Solutions. All chemicals and proteins were purchased from Sigma-Aldrich (Oakville, ON, Canada) unless otherwise stated. Fused silica capillary with an inner diameter of 100 μm and an outer diameter of 360 μm was purchased from Molex Polymicro (Phoenix, AZ) and used throughout this work. His-tagged recombinant Thermus aquaticus MutS protein (MW = 92.8 kDa) was purchased from Prospec (Ness-Ziona, Israel). An Alexa488-labeled MutS-binding aptamer was synthesized by Integrated DNA Technologies (Coralville, IA) and had the following sequence: 5′-Alexa488 CTT CTG CCC GCC TCC TTC CTG GTA AAG TCA TTA ATA GGT GTG GGG TGC CGG GCA TTT CGG AGA CGA GAT AGG CGG ACA CT-3′.[27] Its stock solution was subjected to annealing by incubating at 90 °C for 2 min before cooling it to 20 °C at a rate of 0.5 °C/s, prior to dilution and preparation of equilibrium mixtures. The running buffer (RB) and sample buffer used in both ACTIS and nonequilibrium capillary electrophoresis of equilibrium mixtures (NECEEM) were 50 mM Tris-acetate pH 8.2 supplemented with 0.05% Triton X-100 to reduce the adsorption of DNA and MutS protein to surfaces of vials, capillaries, and connectors.

COMSOL Virtual Experiments. Computer simulation of ACTIS was conducted with an ACTIS virtual instrument (see Scheme S1 for the geometry) built in COMSOL Multiphysics software and described in detail earlier.[25,26] The dimensions of the virtual components were chosen to be identical to those of the physical ACTIS instrument. The parameters used in the virtual ACTIS experiments were chosen based on the properties of the molecular pair (protein−aptamer complex and unbound aptamer) to be separated by TIS. Most aptamers have a length of 40−80 nucleotides and accordingly have a diffusion coefficient μ_L varying in an approximate range of 50−100 μm²/s.[28,29] The robustness of ACTIS to separation flow rates suggests ACTIS to be robust to the choice of μ_L.[19,25] Hence, to simplify the calculations and reduce the computing time, the upper limit value of 100 μm²/s was chosen as μ_L in all virtual ACTIS experiments. The radius a of the injection/separation capillary was set to be 50 μm. The characteristic time of the transverse diffusion of the ligand (aptamer) was
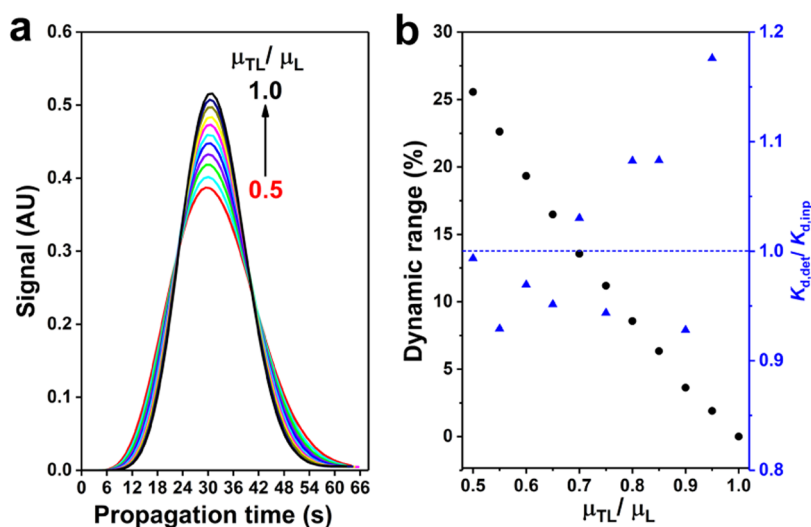
Figure 2. COMSOL simulation: the influence of the ratio between diffusion coefficients of the complex and the ligand (μ_{TL}/μ_L) on (a) the concentration profiles of TL in TIS and (b) the dynamic range of the signal (left axis) and accuracy of K_d determination.

then $\tau_L = a^2/\mu_L = 25$ s. The distance from the point of start of TIS to the detector was set to be 40 cm. The volumetric flow rate for optimal TIS was then calculated as $Q_{TIS} = \pi \mu_L l \approx 8$ μL/min. All other details on COMSOL settings can be found in Note S1.

Poly(vinyl alcohol) (PVA)-Coating. All capillaries used in this work were coated with PVA to reduce the adsorption of sample components to their inner walls. The PVA-coating procedure was modified from our previously published work.[30] PVA (5%, w/v) was prepared by dissolving the polymer in boiling deionized water. Each time, two 130 cm-long capillaries were coated simultaneously. The two uncoated fused silica capillaries were sequentially flushed with 0.1 M NaOH and deionized water for 1 h each under a 6.7 psi flow of nitrogen gas. The pretreated capillaries were then flushed with the PVA solution for 10 min at 8.4 psi and emptied using a 5.6 psi nitrogen gas flow for 10 min. PVA was immobilized on the capillary surface by drying overnight in an oven set at 140 °C and continuously flushed with nitrogen gas at a pressure of 2.8 psi. The detection window on the capillary was made by removing the outer coating with a fuming solution of H_2SO_4.

ACTIS Instrumentation. The ACTIS instrumental setup was identical to the previously published one,[26] except for the following modifications (see schematics in Figure S1). First, the capillary for draining waste was replaced by a 7.0 cm-long "sample aspiration capillary". Second, the sample was introduced into the injection loop by suction: the syringe pump was set at "withdraw only mode" to aspire the sample directly from the sample vial that was placed at the end of the sample aspiration capillary. This modification allowed us not to fill syringes with sample and, thus, avoid adsorption of sample components to the inner wall of syringes. Third, the syringe pump was programmed to only be triggered and run during the injection step allowing for a largely reduced volume of the consumed sample. Finally, the main pump was operated in the "flow-rate-control" mode facilitated by an in-line flow sensor.

ACTIS Experiments. The following changes were made to the previously published ACITS experimental procedure (Figure S1).[26] For step 1, the valve was in position I, and the injection loop was filled with the sample using a syringe pump to aspirate the sample at a flow rate of $Q_s = 50$ μL/min

for 15 s. Since there was a delay for the desired volume of sample to flow through the fluidic path, the valve was set to stay at position I for 40 s. Step 2 was not changed. For step 3, the sample plug was propagated inside the capillary by the main pump at a flow rate of $Q_{TIS} \approx 9$ μL/min for 65 s. For step 4, the separation capillary was rinsed with RB at a flow rate of $Q_{rinse} \approx 37$ μL/min (the highest flow rate we can reach with the current setup) for 2 min, allowing for ~12 volumes of the separation capillary to pass through the fluidic system. The four-step experimental run took ~4.2 min. For the "between-sample" rinsing step, a 1.5 mL sample vial containing RB was placed at the end of the sample aspiration capillary, and the syringe pump was set to continuous withdrawing at a flow rate of 75 μL/min, and the main pump kept injecting the buffer at a flow rate of 37 μL/min. During the "between-sample" rinsing step, the valve was repeatedly switching between positions I and II for 60 times. For each switch, the valve spent 1 s in position I and 2 s in position II. During this rinsing, the buffer with ~37 volumes of the separation capillary passed through the fluidic system. This rinsing step took ~3 min. A total of three ACTIS runs were performed for each concentration of the protein. An ACTIS experiment with seven protein concentrations along with all of the rinsing steps (excluding the sample preparation procedure) took ~3 h. All experiments were conducted at an ambient temperature of 24 ± 1 °C.

Capillary Electrophoresis (CE) Instrumentation. All CE experiments were performed with a P/ACE MDQ apparatus (SCIEX, Concord, Ontario, Canada) equipped with a laser-induced fluorescence (LIF) detection system. Fluorescence was excited with a blue line (488 nm) of a solid-state laser and detected at 520 nm. A 50 cm-long capillary was used (39.8 cm from the inlet to the detector). Prior to each run, the capillary was rinsed with RB at a pressure of 40 psi for 3 min.

NECEEM Experiments. Following the rinsing procedure, the equilibrium mixture was injected into the capillary with a pressure of 0.5 psi for 10 s, which yielded a 1.9 cm-long sample plug. Then, the injected sample plug was propagated through the uncooled region of the capillary at the inlet by injecting a 5.7 cm-long plug of RB with a pressure of 0.3 psi for 50 s. As a result, the total separation distance was 33.2 cm (from the center of the sample plug after its propagation to the detector).

Electrophoretic separation was carried out at 25 kV with an anode at the outlet. The capillary-coolant temperature was set to 15 °C. The duration of electrophoretic separation was 15 min.

■ RESULTS AND DISCUSSION

Virtual Experiments for Complexes with Close μ_{TL} and μ_{L}. As we mentioned, ACTIS is a deterministic method allowing for virtual ACTIS experiments to be conducted *in silico*. Therefore, we used *in silico* experiments to reasonably predict if ACTIS was suitable for the separation of a protein−aptamer complex from unbound aptamer. The ACTIS virtual instrument built in COMSOL was used to study the influence of the ratio between the diffusion coefficient of the target−ligand complex, μ_{TL}, and μ_{L} on the extent of TIS. Since the size of the protein−aptamer complex is larger than that of the unbound aptamer, we can assume that $\mu_{TL} < \mu_{L}$. It is unlikely though that the hydrodynamic radius of the complex is more than twice that of the aptamer. Since the diffusion coefficient depends on the radius reciprocally,[31] the diffusion coefficient of the complex is smaller than that of the aptamer by less than a factor of 2. Hence, we conducted this study for μ_{TL}/μ_{L} ranging from 0.5 to 1 (with a step size of 0.05). Technically, we ran 11 species with distinguishable diffusion coefficients at identical concentrations in COMSOL.

First, we studied TIS concentration profiles under ideal conditions of no noise. The concentration profiles clearly differ (Figure 2a), suggesting that species with such small differences in diffusion coefficient can be separated by TIS. The dynamic range of the signal (see Figure S2 for a sample calculation of dynamic range) decreases with increasing μ_{TL}/μ_{L} (Figure 2b, left axis). This decrease suggests a priori that the robustness of ACTIS to any noise will worsen with increasing μ_{TL}/μ_{L}.

We then ran virtual ACTIS experiments to determine K_{d} values for the same range of variation of μ_{TL}/μ_{L} from 0.5 to 1 with a step of 0.05 (see Figure S3). The dependence of the ratio of determined K_{d} ($K_{d,det}$) to the input value ($K_{d,inp}$) on μ_{TL}/μ_{L} is shown in Figure 2b, right axis. According to the results, the percentage difference between the determined and input K_{d} was within 10% (i.e., $0.9 \leq K_{d,det}/K_{d,inp} \leq 1.1$) for $\mu_{TL}/\mu_{L} \leq 0.9$ but increased rapidly to 18% with μ_{TL}/μ_{L} increasing to 0.95. This decrease of the accuracy was associated with the noise in the simulated signal, which was caused by the finite mesh size of the iterative simulation. Decreasing the mesh size expectedly resulted in decreasing this deviation (see Figure S4).

The above simulations only confirmed what was clear for us *a priori*: ACTIS could be used for K_{d} determination for any finite difference between μ_{TL} and μ_{L} provided that the conditions are ideal. Real ACTIS experiments inevitably have three sources (or two types) of nonideality: instability in flow rate, instability in detector response (low-frequency noise), and detector's high-frequency noise.[26] Reliable K_{d} measurements require that signal variations caused by these non-idealities be much smaller (e.g., $\leq 10\%$) than the dynamic range of the signal. This requirement is a challenge for small differences between diffusion coefficients of TL and L. For instance, the signal dynamic range is only ∼2% for the 5% difference in diffusion coefficients ($\mu_{TL} = 0.95\mu_{L}$; Figure 2b). In this case, reliable K_{d} measurements would require that all of the instabilities and variations be ≤0.2%, which is hardly achievable. This example emphasizes the need for a highly stable ACTIS instrument as well as high-quality ACTIS

experimentation for target−ligand pairs with small differences between μ_{TL} and μ_{L}.

Instabilities in a representative physical ACTIS setup have been recently studied in detail.[26] Instrumental low-frequency variations in the flow rate and detector response were found to cause a run-to-run signal variation (RSD) of ∼2%. Relative noise of the detector (high frequency) should be considered separately from these variations as unlike them it depends on the signal value, which, in turn, is inversely proportional to $[L]_0$. In general, accurate K_{d} measurements require that $[L]_0 < K_{d}$.[32] Since K_{d} is unknown *a priori*, it is preferable to use as low as possible $[L]_0$. However, since decreasing $[L]_0$ leads to a decreasing signal-to-noise ratio (S/N), $[L]_0$ should be chosen such that it balances between measuring low K_{d} values accurately and maintaining reasonably high S/N that is tolerant to experimental errors. In our case, the lowest $[L]_0$ that satisfies the above criteria was 0.05 nM, which produced an S/N of ∼1000, which, in turn, results in a high-frequency noise of 0.1%. Since variations from different sources are additive, the total noise caused by the ACTIS instrument was ∼2%.

In a complete ACTIS experiment with a set of target concentrations $[T]_0$, the potentially largest source of sample-to-sample signal variation is the variation of $[L]_0$ caused by pipetting errors. This variation can be greatly minimized using a procedure for the preparation of a series of equilibrium mixtures described in Note S2. We proved experimentally that, in one titration experiment, our procedure of equilibrium mixture preparation did not contribute detectably to signal variation from all of the other sources since the overall RSD of the diffusive peak intensities in the mock titration was ∼2% (Figure S6). In the future, the accuracy of sample preparation can be further increased using an autosampler.[33] To test how the described sources of variations influence the accuracy of K_{d}, we incorporated the experimental errors, which affect an ACTIS experiment performed with a single set of solutions without changing instrumental settings into our virtual ACTIS instrument.

The two types of variations that we added to the virtual instrument were (i) low-frequency noise of random run-to-run variation of the flow rate with an RSD of 1%, which caused a 2% variation for the signals and (ii) high-frequency detection noise of 0.1% of the signal. We then used this setup to run virtual ACTIS experiments with μ_{TL}/μ_{L} values varying from 0.5 to 1 with a step of 0.05. The separagrams and binding isotherms can be found in Figure S7, while Figure 3 shows the deviation of the determined K_{d} value from the input one as a function of μ_{TL}/μ_{L}. The accuracy of K_{d} determination decreases with decreasing the difference between μ_{L} and μ_{TL}.

If we select a 20% error in K_{d} (i.e., $0.8 \leq K_{d,det}/K_{d,inp} \leq 1.2$) as the highest acceptable deviation, then the smallest acceptable difference between μ_{L} and μ_{TL}, based on data (Figure 3), is ∼15%. We can roughly estimate the smallest size of the protein that can support such a difference between μ_{L} and μ_{TL} since the 15% difference in diffusion coefficients requires a 15% difference in the hydrodynamic radii of L and TL. Assuming the globular geometry of all species, we can convert the 15% (factor of 1.15) difference in radii into a 50% ($1.15^3 \approx 1.5$) difference in the volume or molecular weight (also assuming the same mass density for all species). An 80-nt aptamer has a molecular weight of ∼25 kDa, suggesting the protein of roughly 12.5 kDa as the smallest suitable target. Of course, shorter aptamers would allow working with smaller
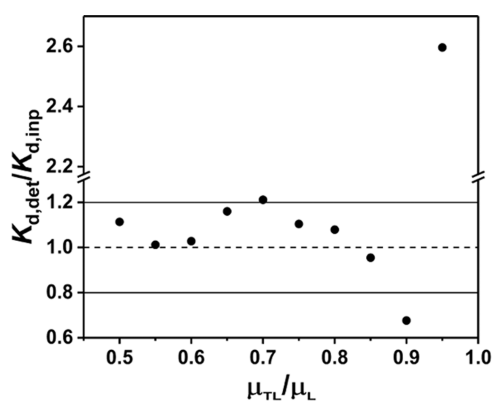
Figure 3. Dependence of the accuracy of K_d determination in virtual ACTIS experiments (with added variations in key parameters describing the virtual instruments) on the ratio between diffusion coefficient, μ_{TL}/μ_L. The solid lines represent a 20% deviation from the input K_d value.

proteins. Overall, the results of our *in silico* experiments suggest the applicability of ACTIS to K_d determination of protein–aptamer complexes, prompting us to the experimental proof of principle.

ACTIS-Based Determination of K_d for MutS–Aptamer Complex. The molecular pair to study experimentally was His-tagged MutS protein (molecular weight of ~93 kDa) as a target and a fluorescently labeled 80-nt ssDNA aptamer selected for a tagless MutS protein as a ligand (the tagless MutS is no longer commercially available).[34] We chose MutS–aptamer as our model pair in this proof-of-principle work for three reasons. First, the MutS—aptamer pair has a diffusion coefficient of less than an order of magnitude and had been previously studied by our lab with a well-established method,[35] which suggested that we could provide a reference study for this molecular pair. Second, this protein–ligand pair was challenging due to its low K_d value and presented an opportunity to prove the suitability of our sample preparation procedure and the high sensitivity of our instrumental detection system. Third, our preliminary study showed a high level of absorptivity of His-tagged MutS to surfaces (e.g., the inner walls of fused silica capillaries). Working with a highly adsorbing protein gave us a chance to optimize our experimental procedure and instrument to apply ACTIS to a broad range of protein targets in the future.

MutS–aptamer was shown to tightly bind the tagless MutS with a K_d = 0.12 nM.[35] Although the affinity of this aptamer to the His-tagged MutS has not been studied, we presumed that the His tag would not affect the binding much, though we did not know the exact K_d value of the complex of this aptamer with the His-tagged MutS a priori. In this case, the aptamer concentration of $[L]_0$ = 0.05 nM was used as a default concentration for all experiments since this concentration was supposed to satisfy the condition of $[L]_0 < K_d$ provided that the tag did not improve the binding much. The molecular weight of the MutS–aptamer complex was calculated to be 118 kDa. Based on the relation between molecular weight and diffusion coefficient mentioned above, μ_{TL}/μ_L was predicted to be ~0.6 ($\sqrt[3]{25}/\sqrt[3]{118}$).

Our first experimental goal was to test if TIS of the MutS–aptamer complex from the unbound aptamer could be detected. For this purpose, in the positive control experiment, we chose the concentration of MutS of 10 nM, which is much greater than the expected K_d value of 0.12 nM and should guarantee that $[TL]_{eq} \gg [L]_{eq}$ in the equilibrium mixture. We thus used an equilibrium mixture of 10 nM MutS and 0.05 nM aptamer for this TIS assessment (Figure 4a). In a negative control experiment, we used an equilibrium mixture of 10 nM BSA and 0.05 nM aptamer (Figure 4b). Every sample was run in triplicate. Adding MutS to the aptamer resulted in the decrease of the diffusive peak, while adding BSA to the aptamer did not change the separagram. It is instructive to note that TIS resulted in a noticeable decrease of the diffusive peak without producing an apparent nondiffusive peak, which was consistent with the prediction in the virtual experiments (see Figure S7, for example). The ratio between the overall noise (i.e., 2%) and the dynamic range of the signal (i.e., ~20%) was ~10%, which established a good ground for the ACTIS-based determination of K_d.

In general, building a binding isotherm for the accurate K_d determination requires that the range of target concentrations extends from much below to much higher than the K_d value. As mentioned above, our expectation was that the K_d for our complex between the aptamer and His-tagged MutS would not differ much from K_d = 0.12 nM determined for the complex of this aptamer with the tagless MutS. Accordingly, we chose the range of target concentration in the equilibrium mixtures to be 3 orders of magnitude from 0.01 to 10 nM, and the constant concentration of the aptamer was 0.05 nM in all mixtures.
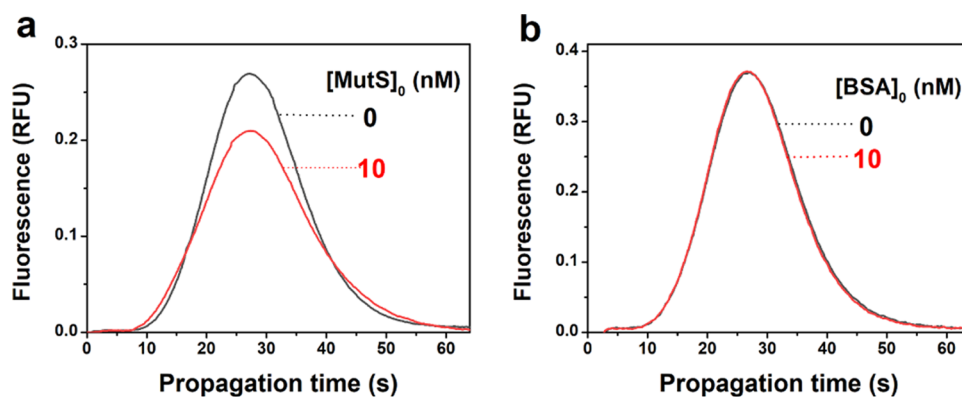
Figure 4. Positive control (a) and negative control (b) for the TIS of MutS–aptamer complex from the unbound aptamer. In the positive control experiment, the aptamer concentration was kept at 0.05 nM, and the concentrations of added MutS protein were 0 and 10 nM. In the negative control experiment, the aptamer concentration was kept at 0.05 nM, and the concentrations of added BSA protein were 0 and 10 nM.
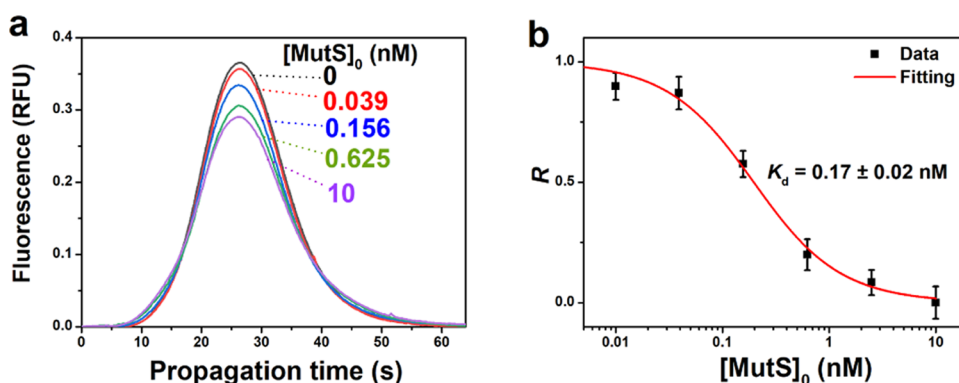
Figure 5. ACTIS-based K_d determination for the MutS−aptamer complex: (a) representative separagrams at different protein concentrations; (b) binding isotherm and curve fitting (using nonlinear regression) to determine K_d. The aptamer (ligand) concentration was kept at 0.05 nM, and the MutS (target) concentration was varied from 0 to 10 nM.
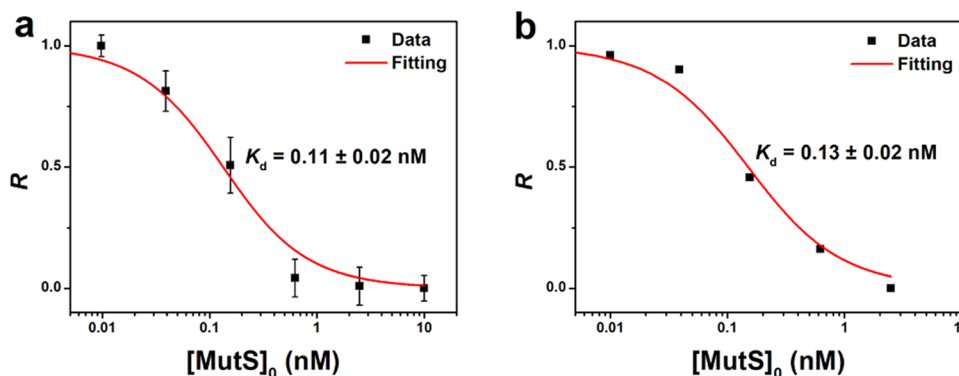
Figure 6. Parallel determination of K_d of the MutS−aptamer complex using ACTIS (a) and NECEEM (b). Binding isotherms and their best nonlinear-regression fits are shown.

Every equilibrium mixture was run in triplicate. Figure 5 shows representative separagrams at different protein concentrations (panel a) and the binding isotherm (panel b). The resulting value of K_d was 0.17 ± 0.02 nM. This experiment was repeated another time on a different day with new equilibrium mixtures (prepared with the same stock protein solution that was used in the 1st day's experiment). The resulting K_d value was 0.19 ± 0.05 nM, which was equal to the first value within the limits of experimental error.

The comparison of separagrams obtained in virtual TIS for varying μ_{TL}/μ_L (Figure 2a) with separagrams obtained in real TIS for saturating target concentrations (e.g., for $[MutS]_0 = 10$ nM in Figure 5) allows us to estimate μ_{TL}/μ_L for the MutS−aptamer pair. The details of this comparison can be found in Figure S11. By comparing the dynamic ranges obtained from virtual and real experiments, the μ_{TL}/μ_L value for the MutS−aptamer pair was found to be 0.6, which was consistent with our prediction.

Comparison of ACTIS with NECEEM. While ACTIS has been proven to be intrinsically accurate, we decided to confirm its result by using another solution-based method: NE-CEEM.[36] NECEEM is a well-established method with well-understood limitations.[37] The quality of separation in NECEEM is, in general, better than in ACTIS (NECEEM can provide baseline separation of the unbound aptamer from the protein-bound aptamer). On the downside, NECEEM separation is much longer (~10 min) than ACTIS separation (<1 min), and accordingly much more prone to the adsorption of T, L, and TL onto the capillary walls. In addition, NECEEM

is incompatible with electrophoresis-unfriendly buffers,[36,38−40] while ACTIS separation does not depend on the ionic composition of the buffer. Another limitation of NECEEM is that electrophoresis generates Joule heat, which makes temperature control an issue.[41−44] ACTIS is a pressure-driven technique with no heat generation in the capillary.

To make the results of ACTIS and NECEEM experiments fully comparable, we conducted NECEEM measurements in parallel with ACTIS measurements using the same equilibrium mixtures. A new stock of MutS solution (different from the one used in the previous 2-day experiment) was used in the sample preparation. As NECEEM separation is much longer than ACTIS separation, we only conducted one run of NECEEM for each equilibrium mixture in contrast to three ACTIS runs for each equilibrium mixture. The resulting binding isotherms are shown in Figure 6. The K_d values obtained were 0.11 ± 0.02 nM with ACTIS and 0.13 ± 0.02 nM with NECEEM. These two values were considered as consistent within the uncertainty range, which confirmed the accuracy of ACTIS in K_d determination for protein−aptamer complex. However, these results differ beyond experimental errors from the ACTIS results obtained in the previous 2-day experiment. We ascribe this inconsistency to hardly avoidable variations in sample preparation. For instance, compared to an older protein stock solution, the newer protein stock solution could have a higher concentration of active protein, which could lead to a lower determined K_d. In addition, at a low protein concentration (i.e., <10 nM), the effects from pipetting errors and protein adsorption are always non-negligible.

According to the results obtained in ACTIS experiments performed on 3 separate days, the weighted average K_d value for His-tagged MutS−aptamer was calculated to be 0.14 ± 0.01 nM (Note S3), which was almost equal to $K_d = 0.12$ nM determined with the tagless MutS protein. This similarity in K_d values for tagged and tagless MutS confirmed that the His tag did not affect the aptamer-binding domain of the protein.

It is important to note that the total areas under the curves in NECEEM experiments with different MutS concentrations (and thus different $[TL]_{eq}/[L]_{eq}$ ratios) were identical within the limits of 5% error without any apparent trend (Table S1). The constancy of the areas indicates that the fluorescence label on the aptamer does not change its quantum yield upon aptamer's binding to MutS. This, in turn, proves that the signal decrease observed in our ACTIS experiments for MutS−aptamer (Figure 4a, for example) was caused by TIS instead of quenching. Overall, the above experimental results are the first and convincing demonstration that ACTIS can be used for the K_d determination of protein−aptamer complexes.

We applied ACTIS to measure K_d of another molecular pair with single-stranded DNA binding protein (SSB, MW = 76 kDa) as the target and a fluorescently labeled 22-nt long ssDNA as a ligand. The K_d values of SSB−22-nt ssDNA were determined to be 16 ± 4 and 15 ± 4 nM in 2 different days (see the representative separagrams and binding isotherms in Figure S15). The consistency of the determined K_d values confirmed the capability of ACTIS to determine K_d values of complexes with small μ_L/μ_{TL}.

CONCLUDING REMARKS

To conclude, we proved that, counterintuitively, a small difference between diffusion coefficients of protein−aptamer complexes and unbound aptamers can result in sufficient TIS to determine K_d accurately. This accuracy was confirmed by the well-studied solution-based method of NECEEM. Method performance in ACTIS will improve with decreasing μ_{TL}/μ_L, i.e., with decreasing size of an aptamer and/or increasing size of the protein. Rough estimates suggest a lower limit of the protein size to be 12.5 kDa for an 80-nt aptamer. In this proof-of-concept study, we used His-tagged MutS (∼93 kDa) and 80-nt long aptamer. In a 3-day ACTIS experiment, the weighted average K_d value for MutS−aptamer was determined to be 0.14 ± 0.01 nM, which was consistent with the previous measurements and served as cross-validation. The variance of the K_d values determined on different days was mainly due to errors in sample preparation. This proof-of-principle work demonstrates that ACTIS with fluorescence detection is applicable to measuring K_d for protein−aptamer pairs accurately and, due to its accuracy, is a potential candidate for a reference K_d-determination method for such binding pairs. ACTIS can potentially be used as a reference method for all molecular complexes (e.g., protein−protein), though every new application needs to be proven experimentally.

ASSOCIATED CONTENT

Supporting Information

The Supporting Information is available free of charge at https://pubs.acs.org/doi/10.1021/acs.analchem.2c03313.

Detailed settings for COMSOL simulations (Note S1); procedure for the preparation of a series of equilibrium mixtures (Note S2); calculation of a weighted average K_d value of the MutS−aptamer complex (Note S3); optimized ACTIS instrumentation and experimental procedure (Figure S1); sample calculation for dynamic range (Figure S2); the virtual experiments with varied μ_{TL}/μ_L without noise (Figure S3); the virtual experiment with a reduced simulation mesh size (Figure S4); repeatability of the ACTIS separagrams for the mock titration experiment (Figure S5); analysis of the results of the ACTIS-based mock titration experiment (Figure S6); the virtual experiments with varied μ_{TL}/μ_L with added experimental noises (Figure S7); repeatability of the ACTIS separagrams for the MutS−aptamer complex, day 1 (Figure S8); repeatability of the ACTIS separagrams for the MutS−aptamer complex, day 2 (Figure S9); ACTIS-based K_d determination for the MutS−aptamer complex, day 2 (Figure S10); estimation of μ_{TL}/μ_L for the MutS−aptamer (Figure S11); repeatability of the ACTIS separagrams for the MutS−aptamer complex in the ACTIS/NECEEM parallel experiment (Figure S12); representative ACTIS separagrams obtained in the ACTIS/NECEEM parallel experiment (Figure S13); electrophoretograms of the NECEEM experiments in the ACTIS/NECEEM parallel experiment (Figure S14); a 2 day ACTIS-based K_d determination for the SSB−22-nt ssDNA complex (Figure S15); and calculation of R values for the NECEEM titration experiment (Table S1) (PDF)

AUTHOR INFORMATION

Corresponding Author

Sergey N. Krylov − *Department of Chemistry and Centre for Research on Biomolecular Interactions, York University, Toronto, Ontario M3J 1P3, Canada;* ⬤ orcid.org/0000-0003-3270-2130; Email: skrylov@yorku.ca

Authors

Tong Ye Wang − *Department of Chemistry and Centre for Research on Biomolecular Interactions, York University, Toronto, Ontario M3J 1P3, Canada;* ⬤ orcid.org/0000-0001-9462-7194

Jean-Luc Rukundo − *Department of Chemistry and Centre for Research on Biomolecular Interactions, York University, Toronto, Ontario M3J 1P3, Canada;* ⬤ orcid.org/0000-0003-3626-2515

An T. H. Le − *Department of Chemistry and Centre for Research on Biomolecular Interactions, York University, Toronto, Ontario M3J 1P3, Canada;* ⬤ orcid.org/0000-0002-3659-9938

Nikita A. Ivanov − *Department of Chemistry and Centre for Research on Biomolecular Interactions, York University, Toronto, Ontario M3J 1P3, Canada;* ⬤ orcid.org/0000-0002-0842-6626

J. C. Yves Le Blanc − *SCIEX, Concord, Ontario L4K 4V8, Canada;* ⬤ orcid.org/0000-0002-3801-3590

Boris I. Gorin − *Eurofins CDMO Alphora, Mississauga, Ontario L5K 1B3, Canada;* ⬤ orcid.org/0000-0003-1500-5392

Complete contact information is available at:
https://pubs.acs.org/10.1021/acs.analchem.2c03313

Notes

The authors declare no competing financial interest.

■ REFERENCES

(1) Fu, H.; Qian, C.; Tong, W.; Li, H.; Chen, D. D. Y. *J. Chromatogr. A* **2019**, *1589*, 182−190.

(2) Wang, N. X.; von Recum, H. A. *Macromol. Biosci.* **2011**, *11*, 321−332.

(3) Schou, C.; Heegaard, N. H. H. *Electrophoresis* **2006**, *27*, 44−59.

(4) Szwajkajzer, D.; Carey, J. *Biopolymers* **1997**, *44*, 181−198.

(5) Ellington, A. D.; Szostak, J. W. *Nature* **1990**, *346*, 818−822.

(6) Tuerk, C.; Gold, L. *Science* **1990**, *249*, 505−510.

(7) Qian, C.; Fu, H.; Kovalchik, K. A.; Li, H.; Chen, D. D. Y. *Anal. Chem.* **2017**, *89*, 9483−9490.

(8) Tang, Z.; Shangguan, D.; Wang, K.; Shi, H.; Sefah, K.; Mallikratchy, P.; Chen, H. W.; Li, Y.; Tan, W. *Anal. Chem.* **2007**, *79*, 4900−4907.

(9) Cooper, M. A. *Nat. Rev. Drug Discovery* **2002**, *1*, 515−528.

(10) Ma, W.; Yang, L.; He, L. *J. Pharm. Anal.* **2018**, *8*, 147−152.

(11) Khavrutskii, L.; Yeh, J.; Timofeeva, O.; Tarasov, S. G.; Pritt, S.; Stefanisko, K.; Tarasova, N. J. *J. Vis. Exp.* **2013**, *78*, No. e50541.

(12) Pan, Y.; Sackmann, E. K.; Wypisniak, K.; Hornsby, M.; Datwani, S. S.; Herr, A. E. *Sci. Rep.* **2016**, *6*, No. 39774.

(13) Krylov, S. N. *SLAS Discovery* **2006**, *11*, 115−122.

(14) Bottari, F.; Daems, E.; de Vries, A.-M.; Wielendaele, P. V.; Trashin, S.; Blust, R.; Sobott, F.; Madder, A.; Martins, J. C.; De Wael, K. *J. Am. Chem. Soc.* **2020**, *142*, 19622−19630.

(15) Yin, A.; Moes, D. J. A. R.; van Hasselt, J. G. C.; Swen, J. J.; Guchelaar, H.-J. *CPT Pharmacometrics Syst. Pharmacol.* **2019**, *8*, 720−737.

(16) Dagan, O.; Bercovici, M. *Anal. Chem.* **2014**, *86*, 7835−7842.

(17) Bahga, S. S.; Bercovici, M.; Santiago, J. G. *Electrophoresis* **2012**, *33*, 3036−3051.

(18) Takahashi, K.; Arjunan, S. N. V.; Tomita, M. *FEBS Lett.* **2005**, *579*, 1783−1788.

(19) Sisavath, N.; Rukundo, J.-L.; Le Blanc, J. C. Y.; Galievsky, V.; Bao, J.; Kochmann, S.; Stasheuski, A. S.; Krylov, S. N. *Angew. Chem., Int. Ed.* **2019**, *58*, 6635−6639.

(20) Chamieh, J.; Leclercq, L.; Martin, M.; Slaoui, S.; Jensen, H.; Østergaard, J.; Cottet, H. *Anal. Chem.* **2017**, *89*, 13487−13493.

(21) Okada, T. *J. Liq. Chromatogr. Relat. Technol.* **2010**, *33*, 1116−1129.

(22) Adrover, A.; Cerbelli, S.; Garofalo, F.; Giona, M. *Anal. Chem.* **2009**, *81*, 8009−8014.

(23) Umehara, R.; Harada, M.; Okada, T. *J. Sep. Sci.* **2009**, *32*, 472−478.

(24) Harada, M.; Kido, T.; Masudo, T.; Okada, T. *Anal. Sci.* **2005**, *21*, 491−496.

(25) Rukundo, J.-L.; Le Blanc, J. C. Y.; Kochmann, S.; Krylov, S. N. *Anal. Chem.* **2020**, *92*, 11973−11980.

(26) Rukundo, J.-L.; Kochmann, S.; Wang, T. Y.; Ivanov, N. A.; Le Blanc, J. C. Y.; Gorin, B. I.; Krylov, S. N. *Anal. Chem.* **2021**, *93*, 11654−11659.

(27) Drabovich, A. P.; Berezovski, M.; Okhonin, V.; Krylov, S. N. *Anal. Chem.* **2006**, *78*, 3171−3178.

(28) Qian, S.; Chang, D.; He, S.; Li, Y. *Anal. Chim. Acta* **2022**, *1196*, No. 339511.

(29) Nkodo, A. E.; Garnier, J. M.; Tinland, B.; Ren, H.; Desruisseaux, C.; McCormick, L. C.; Drouin, G.; Slater, G. W. *Electrophoresis* **2001**, *2424*, 32.

(30) de Jong, S.; Krylov, S. N. *Anal. Chem.* **2012**, *84*, 453−458.

(31) Edward, J. T. *J. Chem. Educ.* **1970**, *47*, 261−270.

(32) Jarmoskaite, I.; AlSadhan, I.; Vaidyanathan, P. P.; Herschlag, D. *eLife* **2020**, *9*, No. e57264.

(33) Tehranirokh, M.; den Bronk, M. V.; Smith, P.; Dai, Z.; Ragunathan, K.; Muscalu, A.; Mills, S.; Breadmore, M. C.; Shellie, R. A. *J. Chromatogr. A* **2021**, *1642*, No. 462032.

(34) Drabovich, A.; Berezovski, M.; Krylov, S. N. *J. Am. Chem. Soc.* **2005**, *127*, 11224−11225.

(35) Kanoatov, M.; Galievsky, V. A.; Krylova, S. M.; Cherney, L. T.; Jankowski, H. K.; Krylov, S. N. *Anal. Chem.* **2015**, *87*, 3099−3106.

(36) Berezovski, M.; Drabovich, A.; Krylova, S. M.; Musheev, M.; Okhonin, V.; Petrov, A.; Krylov, S. N. *J. Am. Chem. Soc.* **2005**, *127*, 3165−3171.

(37) Le, A. T. H.; Wang, T. Y.; Krylova, S. M.; Beloborodov, S. S.; Krylov, S. N. *Anal. Chem.* **2022**, *94*, 2578−2588.

(38) Lou, B.; Chen, E.; Zhao, X.; Qu, F.; Yan, J. *J. Chromatogr. A* **2016**, *1437*, 203−209.

(39) Riley, K. R.; Gagliano, J.; Xiao, J.; Libby, K.; Saito, S.; Yu, G.; Cubicciotti, R.; Macosko, J.; Colyer, C. L.; Guthold, M.; Bonin, K. *Anal. Bioanal. Chem.* **2015**, *407*, 1527−1532.

(40) Mironov, G. G.; Okhonin, V.; Khan, N.; Clouthier, C. M.; Berezovski, M. V. *ChemistryOpen* **2014**, *3*, 58−64.

(41) Berezovski, M.; Krylov, S. N. *Anal. Chem.* **2004**, *76*, 7114−7117.

(42) Xuan, X.; Li, D. *J. Chromatogr. A* **2005**, *1064*, 227−237.

(43) Musheev, M. U.; Filiptsev, Y.; Krylov, S. N. *Anal. Chem.* **2010**, *82*, 8637−8641.

(44) Evenhuis, C. J.; Musheev, M. U.; Krylov, S. N. *Anal. Chem.* **2011**, *83*, 1808−1814.

🕮 Recommended by ACS